

# Asymmetric and unidirectional reflection based on spatial Kramers-Kronig relation induced by dipole-dipole interactions in Rydberg atoms

Di-Di Zheng, Yi-Mou Liu, Yan Zhang, and Jin-Hui Wu

*School of Physics and Center for Quantum Sciences,  
Northeast Normal University, Changchun 130024, China*

For tunable control of asymmetric light reflection, we propose a Rydberg atomic system of the optical response varying in space induced by the long-range position-dependent Rydberg dipole-dipole interaction either in the type of self-van der Waals dipole-dipole interaction or the cross Förster-like dipole-dipole exchange interaction. In such a one-dimensional system consisting of a control atomic driven upon the Rydberg state and a homogeneous target atomic ensemble, the non-localized action from the control atom on the target atoms gradually decreases with the distance between the control and target atoms. Our scheme yields a nonlinear correspondence from a finite spectra range to a finite spatial range of susceptibility via the nonlinear characteristics of Rydberg interaction relative to the position. Therefore, the asymmetric reflection can be induced via the spatial modulation on the target ensemble. In particular, the reflection from one direction can be completely suppressed when the absorption and dispersion parts of the susceptibility are modulated to satisfy the spatial Kramers-Kronig relation in an infinite spectral range. The opposite reflection exhibits a band of a small nonzero reflectivity due to the realistic restriction of the cold atomic density of a relatively small value. Thus, via trapping the target atoms in the optical lattice for the Bragg scattering, we enhance the nonzero reflection obviously and retain the directional reflectionlessness.

## I. INTRODUCTION

In recent years, great efforts have been made in the design and realization of asymmetric reflection of the light and unidirectional invisibility, because the special structures obtained have wide application potential for optical filters, sensors, and diodes. However, the reflection property of natural linear optical materials is usually bidirectional and symmetric according to the Lorentz reciprocal theorem [1]. Moreover, in the view of information optics, since the Fourier transform of any real optical potential (refractive index) function is always symmetric, the light propagation in these materials between the forward and backward modes is symmetric [2–4].

Recently, the asymmetric control of lights has been explored based on several unconventional techniques, such as the optical parity-time symmetric media [5–19], the designed non-reflecting dielectric profiles [20–22], transformation optical media [23–26], and supersymmetric optical structure media [27, 28]. However, these media require inevitable regimes of gain or anisotropy, making it challenging in the experimental implementation. In 2015, Horsley *et al.* has found waves propagating through an inhomogeneous medium of specially designed complex permittivity profile, of which the real and imaginary parts are related by the spatial Kramers-Kronig (KK) relation, can be efficiently absorbed from one side of the medium but be normally reflected from the other side [29]. Then, without the requirement of gain and anisotropy, a series of such media satisfying spatial KK relation have been proposed for the unidirectional reflection with the negligible transmission in the theory [30–33] and the experiment [34]. The spatial KK media are designed by the fixed spatial structure and transformation optics [35]. Yet, these schemes have the disadvantage of lacking dynamic tunability due to fixed inhomogeneous

spatial structures of the complex optical response function with the spatial KK profile.

As a tunable quantum scheme, the system involving Rydberg atoms has been widely used in quantum computing [36–40], electromagnetic field sensing [41–43], and quantum optics [44–50]. The main reason is the advantage of the cooperation between the long lifetime of Rydberg states and the coherent control of the interactions between two close Rydberg atoms arising from the large electric dipole moments due to the large atomic size. The strong long-range interaction is regarded as two types, the nonresonant van der Waals dipole-dipole interaction scaling as  $1/R^6$  with the inter-atomic distance  $R$  and the even larger resonant Förster-like dipole-dipole exchange interaction scaling as  $1/R^3$ . The energy interaction is related to the principal quantum number and  $R$  and also can be controlled by the applied external electromagnetic field. As two direct consequences of such position-dependent interactions, one is typically the local dipole blockade effect, *i.e.*, an atom promoted to a Rydberg level can shift the levels of nearby atoms to suppress the excitation of its neighbors onto the Rydberg state [37, 51, 52], and the other is relatively weak finite interaction. Both of them contribute to the realization of the atomic schemes for the controllable photonic grating [53–55] and photonic transistor [56–58]. Here, we would like to use the non-localized Rydberg interaction varying in space to induce the spatial KK modulation on a homogeneous atomic ensemble, and then asymmetrically control the light propagation with such a non-Hermitian atomic system.

With the presence of a position-dependent dipole-dipole interaction, we propose an efficient non-Hermitian atomic scheme involving Rydberg states of  $^{87}\text{Rb}$  atoms for mapping the usual KK relation of the probe susceptibility from the frequency domain into the space do-

main. Such a one-dimension (1D) system is composed of a target Rydberg atomic ensemble and a control Rydberg atom, which is strongly pumped upon the Rydberg state and then kept in a dark state to yield a nearly perfect Rydberg excitation. The control atom can act on the target atoms via two kinds of dipole-dipole interactions. By substituting either of two kinds of dipole-dipole potential into the probe susceptibility of the target ensemble, the system of the space-varying susceptibility is found to exhibit asymmetric reflection and even unidirectional reflectionlessness in the regime of the well-satisfied spatial KK relation. In addition, when trapping the KK-modulation target atoms into an optical lattice for the introduction of the Bragg scattering, the nonzero reflectivity can be dramatically enhanced by orders of magnitude with maintaining the unidirectional vanishing reflectivity. With such an incorporation between the spatial KK modulation based on Rydberg interaction and the periodic spatial modulation, an effective and tunable scheme of unidirectional reflection can be realized, which is expected to be used for the photonic router and transistor.

## II. MODEL AND EQUATIONS

Our  $^{87}\text{Rb}$  Rydberg atomic level configuration is shown in Fig. 1(a,b). The control atom denoted by A3 is in the three-level ladder configuration with a ground state  $|1\rangle$ , an excited state  $|2\rangle$  and a Rydberg state  $|3\rangle$  with rate  $\Gamma_{32}$ , where the transition  $|1\rangle \leftrightarrow |2\rangle$  is resonantly pumped by the strong field of frequency  $\omega_1$  and amplitude  $E_1$  and the transition  $|2\rangle \leftrightarrow |3\rangle$  by the strong field of frequency  $\omega_2$  and amplitude  $E_2$ . We consider the target atoms with a ground state  $|g\rangle$  and a Rydberg state  $|r\rangle$  with rate  $\Gamma_{re}$ , are driven in two cases denoted by T3, 2, respectively, in Figs. 1(a) and (b). In (a), the target atoms T3 are coupled into the three-level ladder type with an extra excited state  $|e\rangle$ , where the lower (upper) transition  $|g\rangle \leftrightarrow |e\rangle$  ( $|e\rangle \leftrightarrow |r\rangle$ ) of resonant frequency  $\omega_{eg}$  ( $\omega_{re}$ ) is coupled by a weak probe field of frequency  $\omega_p$  and amplitude  $E_p$  (a strong coherent field of frequency  $\omega_c$  and amplitude  $E_c$ ). In (b), the target atoms T2 are coupled into the two-level type in the absence of  $E_c$ , where a weak probe field of frequency  $\omega_p$  and amplitude  $E_p$  directly acts upon the transition  $|g\rangle \leftrightarrow |r\rangle$  of resonant frequency  $\omega_{rg}$ . For A3, the Rabi frequencies  $\Omega_1 = E_1 \cdot \wp_{21}/2\hbar$  and  $\Omega_2 = E_2 \cdot \wp_{32}/2\hbar$ ; for T3, the corresponding detunings  $\Delta_p = \omega_{eg} - \omega_p$  and  $\Delta_c = \omega_{re} - \omega_c$ , and the Rabi frequencies  $\Omega_p = E_p \cdot \wp_{eg}/2\hbar$  and  $\Omega_c = E_c \cdot \wp_{re}/2\hbar$ ; for T2, the corresponding detuning  $\Delta_p = \omega_{rg} - \omega_p$  and the Rabi frequency  $\Omega_p = E_p \cdot \wp_{rg}/2\hbar$ . Here,  $\wp_{ij}$  denotes electric dipole moments on transition  $|i\rangle \rightarrow |j\rangle$ , while  $\Gamma_{21}$ ,  $\Gamma_{32}$ ,  $\Gamma_{re}$ , and  $\Gamma_{eg}$  describe the population decay rates between the relevant states, respectively.

These atoms are distributed along the one-dimensional  $x$ -axis. A3 is on the origin of the  $x$ -axis, and the target atomic ensemble of length  $L$  has a homogeneous atomic number density in Fig. 1(c) or a periodical density dis-

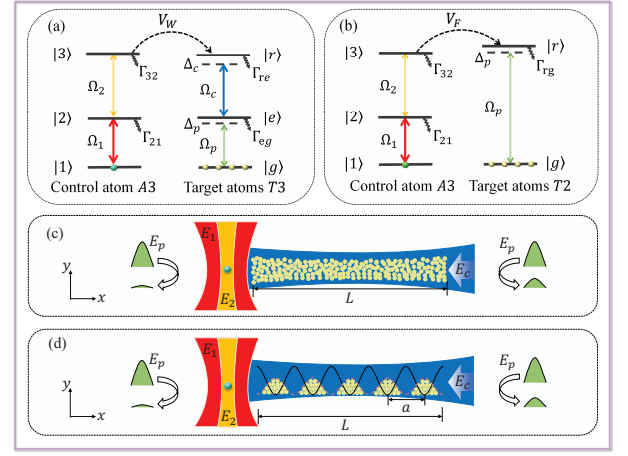


FIG. 1: (a) and (b) Atomic level schemes where the control atom A3 is driven by two strong pump fields  $\Omega_1$  and  $\Omega_2$  into the three-level ladder configuration. In (a), the three-level ladder-type target atoms T3 are coupled by a weak probe field  $\Omega_p$  and a strong coherent field  $\Omega_c$ , and then two high Rydberg states  $|3\rangle = |r\rangle$  exhibit the van der Waals dipole-dipole interaction with potential  $V_W$ ; In (b), the two-level target atoms T2 are probed by a weak field ( $\Omega_p$ ) and two high Rydberg states  $|3\rangle \neq |r\rangle$  interact via the Förster-like dipole-dipole exchange interaction with potential  $V_F$ . (c) and (d) Schematic of the coherent interaction between external light fields and cold atoms system. A control atom A3 illuminated by two pumping laser fields of amplitudes  $E_{1,2}$  along the  $y$ -axis, is located at the origin of the  $x$ -axis, while the target atoms T3 or T2 on the  $+x$ -axis from  $x = 0$  to  $L$  are exposed to a strong coherent field of amplitude  $E_c$  along the  $x$ -axis. The probe field  $E_p$  is input either along the  $+x$  or  $-x$  direction. In (c) The target atomic ensemble is of homogeneous density; in (d) target atoms are loaded into a one-dimension optical lattice (black solid curve) of period  $a$  when being trapped at the bottom of dipole traps with a Gaussian distribution in a unit cell.

tribution in Fig. 1(d). The pump fields  $E_{1,2}$  illuminate A3 along  $y$ -axis. The coherent field  $E_c$  illuminates T3 along  $x$ -axis, and the probe field  $E_p$  is input either along  $+x$  or  $-x$  direction. For using two different dipole-dipole interactions,  $|3\rangle = |r\rangle \equiv |nS_{1/2}\rangle$  in Fig. 1(a) for the nonresonant van der Waals dipole-dipole interactions between A3 and T3, and  $|3\rangle \equiv |nS_{1/2}\rangle$  and  $|r\rangle \equiv |nP_{3/2}\rangle$  in Fig. 1(b) for resonant Förster-like dipole-dipole exchange interactions between A3 and T2. Note that,  $\Omega_1$  and  $\Omega_2$  are much larger than  $\Omega_c$  and  $\Omega_p$  so that A3 is always on the Rydberg state with the approximate neglect of the reaction from T3 or T2. Then, under the rotating-wave and electric-dipole approximations, Hamiltonians of A3, T3 and T2 are, respectively,

$$\hat{H}_{A3} = -\hbar(\Omega_2\hat{\sigma}_{32} + \Omega_1\hat{\sigma}_{21} + \Omega_2^*\hat{\sigma}_{23} + \Omega_1^*\hat{\sigma}_{12}), \quad (1a)$$

$$\hat{H}_{T3} = -\hbar[-(\Delta_p + \Delta_c)\hat{\rho}_{rr} - \Delta_p\hat{\rho}_{ee} + \Omega_c\hat{\rho}_{re} + \Omega_p\hat{\sigma}_{eg} + \Omega_c^*\hat{\sigma}_{er} + \Omega_p^*\hat{\sigma}_{ge} - V_W\hat{\sigma}_{33}\hat{\rho}_{rr}], \quad (1b)$$

$$\hat{H}_{T2} = -\hbar(-\Delta_p\hat{\rho}_{rr} + \Omega_p\hat{\rho}_{rg} + \Omega_p^*\hat{\rho}_{gr} - V_F\hat{\sigma}_{33}\hat{\rho}_{rr}), \quad (1c)$$

where  $\hat{\sigma}_{\mu\nu}$  and  $\hat{\rho}_{ij}$  are the transition operators ( $\mu \neq \nu$ ,  $i \neq j$ ) or the projection operator ( $\mu = \nu$ ,  $i = j$ ) with  $\mu, \nu = 1, 2, 3$  and  $i, j = g, e, r$ . Here,  $\hat{V}_W = (C_6/x^6)\hat{\sigma}_{33} \otimes \hat{\rho}_{rr}$  is the potential arising from the van der Waals interaction, and  $\hat{V}_F = (C_3/x^3)\hat{\sigma}_{33} \otimes \hat{\rho}_{rr}$  from the Förster-like interaction.

The dynamics of system is governed by the master equation  $\partial_t \hat{\rho} = -\frac{i}{\hbar}[\hat{H}, \hat{\rho}] + \mathcal{L}(\hat{\rho})$ , where  $\mathcal{L}(\hat{\rho}) = \sum \Gamma_{\mu\nu}[\hat{\sigma}_{\nu\mu}\hat{\rho}\hat{\sigma}_{\mu\nu} - \frac{1}{2}(\hat{\rho}\hat{\sigma}_{\mu\nu}\hat{\sigma}_{\nu\mu} + \hat{\sigma}_{\mu\nu}\hat{\sigma}_{\nu\mu}\hat{\rho})]$  describing the dissipation processes arising from Rydberg decay rates  $\Gamma_{3,r}$ . It is straightforward to expand Hamiltonians in Eq. (1) into the optical Bloch equation. Then, in the steady state, we can get the required Rydberg state population  $\sigma_{33}$  of A3

$$\sigma_{33} = \frac{(\gamma_{21} + \gamma_{32})\Omega_1^2\Omega_2^2}{(\gamma_{32}\gamma_{31} + \Omega_2^2 + \Omega_1^2)(\gamma_{21}^2\gamma_{32} + \gamma_{21}\Omega_2^2 + 2\gamma_{32}\Omega_1^2)}. \quad (2)$$

Here, the population  $\sigma_{33} \approx 1$  in the presence of the two enough strong resonant-coupling fields  $\Omega_1$  and  $\Omega_2$ . Then, we can achieve the steady-state susceptibilities of the target atoms T2 and T3 by solving the optical Bloch equation in the steady state using the weak field approximation, respectively,

$$\chi_3 = \frac{N_0|\wp_{rg}|^2}{\hbar\epsilon_0} \frac{-i\gamma_{rg} + \Delta_3^{eff}}{(\Delta_p - i\gamma_{eg})(-i\gamma_{rg} + \Delta_3^{eff}) - \Omega_c^2}, \quad (3a)$$

$$\chi_2 = \frac{N_0|\wp_{rg}|^2}{\hbar\epsilon_0} \frac{i}{\gamma_{rg} + i\Delta_2^{eff}}, \quad (3b)$$

with the effective detuning  $\Delta_3^{eff} = \Delta_p + \Delta_c + \delta_x$  ( $\Delta_2^{eff} = \Delta_p + \delta_x$ ), where  $\delta_x = (C_6/x^6) \cdot \sigma_{33}$  ( $\delta_x = (C_3/x^3) \cdot \sigma_{33}$ ) for the susceptibility  $\chi_{T3}$  ( $\chi_{T2}$ ) is the Rydberg energy level shift related to the position induced by the van der Waals dipole-dipole (Förster-like dipole-dipole exchange) interaction. Here,  $N_0$  denotes the average target atomic density. Then, the real part  $\chi'$  and imaginary part  $\chi''$  of the complex susceptibility corresponding to either  $\chi_{T3}$  or  $\chi_{T2}$ , govern the local dispersion and absorption properties around resonance frequency, respectively.

It is apparent that, the denominator of  $\chi_3$  ( $\chi_2$ ) is a linear function of  $\Delta_3^{eff}$  ( $\Delta_2^{eff}$ ) and  $\sigma_{33}$  is constant, so the denominator is inversely proportional to the sixth (third) power of  $x$ . The variation in  $\Delta_3^{eff}$  ( $\Delta_2^{eff}$ ) according to the position-dependent change in shift  $\delta_x$ , is equivalent to the introduction of the spatial variation to the frequency-dependent susceptibility. Then, the susceptibility of target atoms bears the spatial modulation arising from the Rydberg interaction.

As we know, the real part  $\chi'$  and imaginary part  $\chi''$  of both susceptibilities can be related via the KK relation in the frequency domain based on the causality principle and Cauchy's theorem if we set  $\delta_x = 0$  here [59]. Thus, for a appropriate position  $x$  and detuning  $\Delta_p$ , this relation may also hold in the space domain described by

$$\chi'(\Delta_p, x) = \frac{1}{\pi} P \int_0^L \frac{\chi''(\Delta_p, s)}{s - x} ds, \quad (4)$$

where  $P \int_0^L \dots$  indicates the Cauchy principle value integral relevant to the coordinate  $s$ . The systems satisfying such a spatial KK relation are known to not reflect radiation incident from one side due to the perfect absorption, whatever the angle of incidence [29, 60]. That is, under the spatial KK relation, when the field incident from one side can be reflected normally, the opposite real wavevector is forbidden and the corresponding reflected field may vanish as the evanescent wave. Then target atomic ensembles of the susceptibilities in Eq. (4) is expected to exhibit asymmetric light transport characteristics. However, owing to the nonlinear dependence of shift  $\delta_x$  on position  $x$  according to the dipole-dipole interaction potential, the complex susceptibility becomes complicated and then not simply shows the same profile in the space domain as that in frequency domain.

The reflection and transmission spectra of the target atoms can be examined with the help of the transfer matrix method [61]. First, we partition the atomic sample into a large number ( $N$ ) of thin slabs with a thickness  $k$  of each slab, then derive the individual transfer matrix  $M_n$  of the  $n$ th slab with the complex susceptibility, and finally multiply the matrices of all slabs in succession for the total transfer matrix  $M$  of the whole sample. To be specific, we first derive the  $2 \times 2$  unimodular transfer matrix  $M_n(\Delta_p, k)$  describing the dynamics propagation of a field through the  $n$ th slab

$$\begin{bmatrix} E_p^+(\Delta_p, nk) \\ E_p^-(\Delta_p, nk) \end{bmatrix} = M_n(\Delta_p, k) \begin{bmatrix} E_p^+(\Delta_p, (n-1)k) \\ E_p^-(\Delta_p, (n-1)k) \end{bmatrix}, \quad (5)$$

where two complex components  $E_p^+$  and  $E_p^-$  describes forward and backward fields, respectively, while the transformation is

$$M_n(\Delta_p, k) = \frac{1}{t_n} \begin{bmatrix} t_n^2 - r_{nl}r_{nr} & r_{nr} \\ -r_{nl} & 1 \end{bmatrix}, \quad (6)$$

with the corresponding complex transmission amplitude  $t_n$  and reflection amplitude  $r_{nl}$  ( $r_{nr}$ ) for the probe field incident from the left (right) side, determined by the complex refractive index  $n_n = \sqrt{1 + \chi_n}$ . Then, the total transfer matrix turns out to be  $M(\Delta_p, L) = M_1(\Delta_p, k) \cdots M_n(\Delta_p, k) \cdots M_N(\Delta_p, k)$  for atomic sample of length  $L = Nk$ .

Finally, we can obtain the corresponding probe reflectivities  $R_{l,r}$  and transmissivity  $T$  on both sides

$$\begin{aligned} R_l(\Delta_p, L) &= |r_l(\Delta_p, L)|^2 = \left| \frac{M_{(21)}(\Delta_p, L)}{M_{(22)}(\Delta_p, L)} \right|^2, \\ R_r(\Delta_p, L) &= |r_r(\Delta_p, L)|^2 = \left| \frac{M_{(12)}(\Delta_p, L)}{M_{(22)}(\Delta_p, L)} \right|^2, \\ T(\Delta_p, L) &= |t(\Delta_p, L)|^2 = \left| \frac{1}{M_{(22)}(\Delta_p, L)} \right|^2, \end{aligned} \quad (7)$$

in terms of relevant matrix entries of  $M(\Delta_p, L)$ .

TABLE I: The used dipole-dipole coefficient and electric dipole moments

	$( 3\rangle,  r\rangle)$	coefficient $C( 3\rangle,  r\rangle)$	electric dipole moment $\wp$
Fig. 1(a)	$80S_{1/2}, 80S_{1/2}$	$C_6 = -2\pi \times 4.25 \times 10^{12} s^{-1} \mu m^6$	$\wp_{eg} = 1.79 \times 10^{-29} C \cdot m$
Fig. 1(b)	$60S_{1/2}, 60P_{3/2}$	$C_3 = -2\pi \times 0.38 \times 10^{10} s^{-1} \mu m^3$	$\wp_{rg} = 6.21 \times 10^{-32} C \cdot m$

### III. RESULTS AND DISCUSSION

The energy levels and realistic parameters of the cold  $^{87}Rb$  Rydberg atoms are chosen for two kinds of dipole-dipole interactions, *i.e.*, in Fig. 1(a),  $|1\rangle \equiv 5S_{1/2}$ ,  $|2\rangle \equiv 5P_{3/2}$ ,  $|3\rangle \equiv 80S_{1/2}$ ,  $|g\rangle \equiv 5S_{1/2}$ ,  $|e\rangle \equiv 5P_{3/2}$  and  $|r\rangle \equiv 80S_{1/2}$  with  $\Gamma_3/2\pi = \Gamma_r/2\pi = 0.26$  kHz and  $\Gamma_{eg}/2\pi = 5.746$  MHz corresponding to the consequent van der Waals interaction causing the potential  $V_W$  of the dipole-dipole coefficient  $C_6$ ; in Fig. 1(b),  $|1\rangle \equiv 5S_{1/2}$ ,  $|2\rangle \equiv 5P_{3/2}$ ,  $|3\rangle \equiv 60S_{1/2}$ ,  $|g\rangle \equiv 5S_{1/2}$  and  $|r\rangle \equiv 60P_{3/2}$  with  $\Gamma_3/2\pi = 0.63$  kHz and  $\Gamma_r/2\pi = 0.33$  kHz corresponding to the consequent Förster-like dipole-dipole exchange interaction causing the potential  $V_F$  of the dipole-dipole coefficient  $C_3$ . Other relevant parameters used according to refs. [62, 63] are shown in Table I. For the high Rydberg excitation of the control atom  $A3$ , two strong pumping fields are used with  $\Omega_1/2\pi = 50$  MHz,  $\Omega_2/2\pi = 10$  MHz and, in consequence, the Rydberg population  $\sigma_{33} \simeq 0.96$ . Then, the dipole-dipole-interaction induced position-dependent energy shift of  $|r\rangle$  for target atoms can be simplified to  $\delta_x \simeq C_6/x^6$  ( $\delta_x \simeq C_3/x^3$ ) for  $T3$  ( $T2$ ).

#### A. Target atomic ensemble with homogeneous density

We first consider the target atomic ensembles  $T3, 2$  with a homogeneous distribution on the  $+x$  axis as shown in Fig. 1(c). We plot the real and imaginary parts of the complex probe susceptibilities of  $T3$  ( $T2$ ) along  $x$  with different probe detunings  $\Delta_p$  in Fig. 2 (3). In Fig. 2, it is found that the spatial variation in profiles of  $\chi'_3$  and  $\chi''_3$  are induced by the position-dependent van der Waals interaction. For example, for the resonance of  $\Delta_p = 0$  MHz, on the left side of the ensemble, the target atoms near the control atom  $A3$  are suppressed to excite to Rydberg states, and then are retained in a two-level type via the enough large interaction with a small  $x$ ; those on the right side and far from the atom  $A3$  are in the three-level type due to the dramatic decreasing in the interaction scaling as  $1/x^6$  with the increasing  $x$ . As the magenta-squared curves in Fig. 2(b),  $\chi''_3$  shows relative big value near the left side due to the intense absorption of the resonant two-level atoms, and vanishes due to the perfect transparency of the resonant three-level atoms based on the well-known electromagnetically induced transparency.  $\chi'_3$  also implies the corresponding dispersion property of the two-level (three-level) atoms near the left (right) side. In the vicinity of the middle

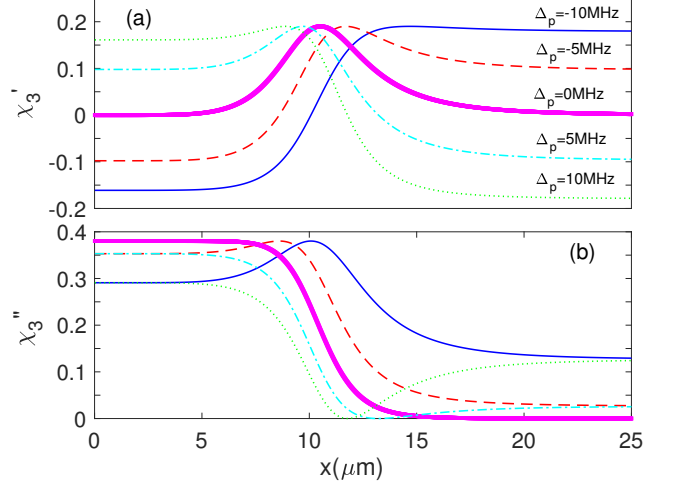


FIG. 2: (a) Real part  $\chi'_3$  and (b) imaginary part  $\chi''_3$  of probe susceptibility  $\chi_3$  of  $T3$  as functions of position  $x$ . The blue-solid, red-dashed, magenta-squared, cyan-dash-dotted, and green-dotted curves are obtained, respectively, with  $\Delta_p = -10$  MHz,  $-5$  MHz,  $0$  MHz,  $5$  MHz, and  $10$  MHz. The wavelength of the probe field is  $\lambda_p = 795$  nm. Other parameters are  $\Omega_c/2\pi = 3.0$  MHz,  $\Delta_c = 0$  MHz,  $N_0 = 2.0 \times 10^{13} \text{ cm}^{-3}$ ,  $L = 25 \mu\text{m}$ .

of the ensemble, the change in the susceptibility is determined by the Rydberg excitation probability of the target atoms, *i.e.*, the mixing proportion between the two-level and three-level atoms. In addition, the profiles of  $\chi'_3$  and  $\chi''_3$  also change with the varying probe detuning  $\Delta_p$ , because the susceptibility is a binary function of the frequency and position. It is interesting that the real part  $\chi'_3$  can change between the even-like profile and odd-like profile with the varying  $\Delta_p$  while the imaginary part  $\chi''_3$  changes oppositely. Those profiles do not show exact even/odd symmetry, however, the definite symmetry under inversion of space is sufficient but unnecessary for the spatial KK relation[29].

Note that, the usual KK relation is that the absorption and dispersion parts of the susceptibility satisfy the KK relation over the entire spectrum. However, after a mapping from the spectral range into the spatial range, if the spectral line is fully contained inside the finite sample, we have the conservative KK relation; otherwise, the KK relation does not hold again. In Fig. 3, the space-varying probe susceptibility for  $T2$  with the position-dependent dipole-dipole exchange interaction, is plotted. The real and imaginary parts of the susceptibility show, respectively, the relatively simple odd and even profiles due to the simple expression as Eq. (3b). The variations

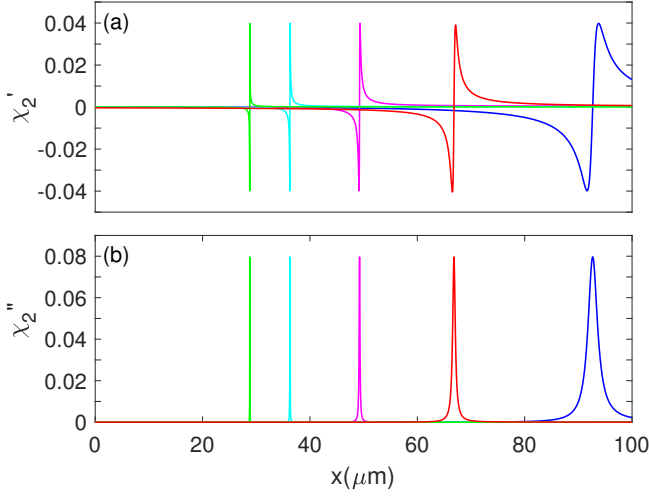


FIG. 3: (a) Real part  $\chi_2'$  and (b) imaginary part  $\chi_2''$  of probe susceptibility  $\chi_2$  of  $T2$  as functions of position  $x$ . From right to left, the blue, red, magenta, cyan, and green curves are obtained, respectively, with  $\Delta_p = 0.03$  MHz, 0.08 MHz, 0.2 MHz, 0.5 MHz and 1 MHz. The wavelength of the probe field is  $\lambda_p = 297$  nm. Other parameters are  $\Omega_c/2\pi = 3.0$  MHz,  $\Delta_c = 0$  MHz,  $N_0 = 2.0 \times 10^{13} \text{ cm}^{-3}$  and  $L = 100 \text{ } \mu\text{m}$ .

in  $\Delta_p$  not only shift the position but also change the width of the susceptibility profile, *i.e.*, the width would decrease sharply with the decreasing of  $x$  that can be showed with Eq. (3b). However, they do not change the profiles of the susceptibility obviously in the space, compared with Fig. 2. In addition, as the detuning  $\Delta_p$  gradually increases, the profile gradually enters into the medium from right, thus, the  $T2$  system will transition from the regime of completely destroyed spatial Kk modulation to the regime of well-satisfied spatial Kk relation

Comparing these two cases of  $T3$  and  $T2$ , the spatial variations in the susceptibilities can be induced by the position-dependent interactions, either the van der Waals interaction or the dipole-dipole exchange interaction. For  $T2$ , the susceptibility of the two-level system can keep a spatial KK profile in the sample within a range of the probe frequency. However, in the case of  $T3$ , the susceptibility of the three-level system is more complicatedly connected to the probe frequency, and thus, the profile of the susceptibility varies more obviously with the frequency and then may not exactly satisfy the spatial KK relation.

In the frequency range where a finite atomic sample contains an obvious susceptibility profile in space, to quantify whether the spatial KK relation is satisfied or not, we propose a criterion  $D_{kk}$  for the spatial KK relation in the finite sample as

$$D_{kk} = \begin{cases} \frac{\int_0^L (\chi''(\Delta_p, x) - \frac{1}{\pi} P \int_0^L \frac{\chi'(\Delta_p, s)}{s-x} ds) dx}{B} & B \neq 0, \\ \int_0^L (\chi''(\Delta_p, x) - \frac{1}{\pi} P \int_0^L \frac{\chi'(\Delta_p, s)}{s-x} ds) dx & B \simeq 0, \end{cases} \quad (8)$$

where  $B = |\int_0^L \chi''(\Delta_p, x) dx|$ . Here,  $D_{kk} \simeq 0$  denotes

the unbroken regime where the spatial KK relation is satisfied, which means a KK profile of susceptibility is completely contained by the sample.  $D_{kk} > 0$  denotes the broken regime where the spatial KK relation is destroyed, which means the profile of susceptibility partially leave the sample.

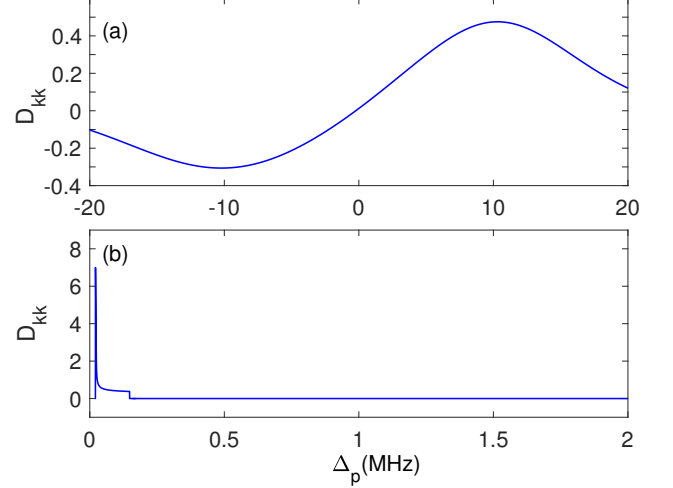


FIG. 4: Figure of merit  $D_{kk}$  against detuning  $\Delta_p$  for  $T3$  in (a) with parameters as in Fig. 2; for  $T2$  in (b) with parameters as in Fig. 3.

In Fig. 4(a) and (b), we plot the figure of merit  $D_{kk}$  for  $T3$  and  $T2$ , respectively. In Fig. 4(a), there is only one point of  $D_{kk} = 0$  near the resonance ( $\Delta_p = 0$  MHz), which means the susceptibility of  $T3$  can satisfy the spatial KK relation just at a frequency point. In Fig. 4(b), there is a narrow band of frequency for  $D_{kk} \simeq 0$ . Such a frequency-dependent spatial modulation on the probe susceptibility is different from the previous works on the spatial KK relation [30, 34, 64–69], where the design of medium is fixed in the absence of dynamic spatial modulation, *i.e.*, not tunable.

Then, we plot the reflections  $R_l$  ( $R_r$ ) of the probe fields incident from the left (right) side for the ensembles  $T3$  and  $T2$ , respectively, in Fig. 5(a) and (b). In Fig. 5(a), the left reflection is completely suppressed at the point  $\Delta_p = 0$  MHz corresponding to  $D_{kk} = 0$  when the probe field incident from the right side is normally reflected, which means the unidirectional reflection is realized. In the other frequency range of the transition regime of the spatial KK relation, both reflections are nonzero but distinct, which means the asymmetric reflection appears. As the reflection spectrum shown in Fig. 5(b) in the corresponding range of  $D_{kk} \simeq 0$  in Fig. 4(b), the right reflection vanishes and the left reflection appear with the varying nonzero reflectivity. Results show that, due to the dependence on the position, the Rydberg dipole-dipole interaction can spatially modulate the probe susceptibility of the target atomic ensemble. Thus, the target atoms with a space-varying susceptibility can show the asymmetric reflection. Especially, the unidirec-



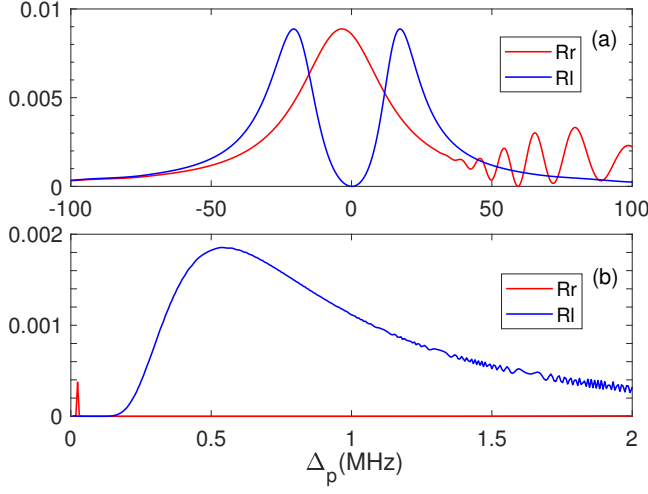


FIG. 5: Reflectivities  $R_l$  (red curves) and  $R_r$  (blue curves) against detuning  $\Delta_p$  (a) for  $T3$  in (a) with parameters as in Fig. 2; for  $T2$  in (b) with parameters as in Fig. 3.

tional reflection can be obtained when the system is in the regime of spatial KK modulation.

### B. Target atomic ensemble trapped in a lattice

Although, within the proper probe frequency range/point, both  $T3$  and  $T2$  can exhibit unidirectional reflectionless features, the maximum reflectivity of the unidirectional reflection is not large enough due to the realistic cold atomic parameters. For enhancing the nonzero reflectivity in the unbroken KK-relation regime, We load these target cold atoms in a 1D optical lattice of period  $a$  to create a periodic atomic density  $N(x)$  in the space, as shown in Fig. 1(d).

In the  $j$ th unit cell of such a lattice, the trapped target atoms have a Gaussian density distribution as

$$N_j(x) = N_0 e^{-(x-x_j)^2/d_x^2}, \quad (9)$$

with  $d_x$  being the width of the atomic distribution in a cell at the location of center  $x_j = (j - 1/2) \times a$ . Here we use  $N_0 = 2.0 \times 10^{13} \text{ cm}^{-3}$  and  $\delta_x = a/6$ . Thus, we combine the periodic spatial modulation of Bragg scattering with the inhomogeneous spatial KK modulation for the larger nonzero reflectivity of the unidirectional reflection. First, we plot the real and imaginary parts of the probe susceptibility for atomic lattices of  $T3$  and  $T3$  in Fig. 6.

Because we use the same parameters here as before, as shown in Fig. 6, both the real and imaginary parts of susceptibilities exhibit the same profiles as those in Figs. 2 and 3 except the comb-like spatial variations according to the periodic structure of the atomic lattices. Thus, the frequency range/point of the unbroken KK relation for the lattice system may be similar to before, but the change in nonzero reflectivity may be obvious.

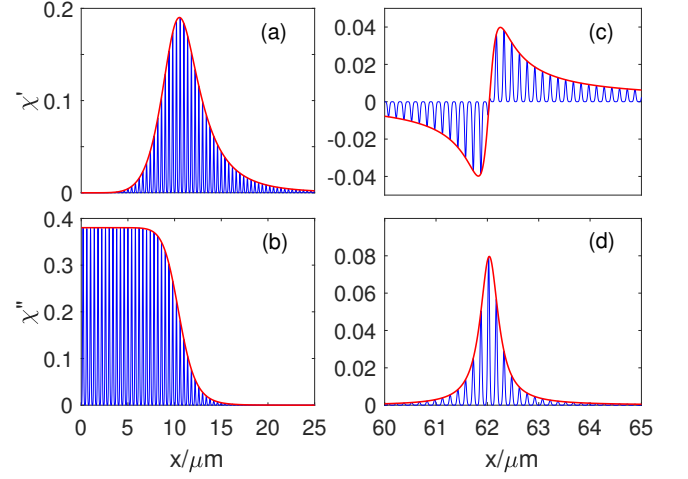


FIG. 6: (a) Real part  $\chi'_3$  and (c) part  $\chi''_3$  of the susceptibility for  $T3$  trapped as an atomic lattice of a period  $a = 400 \text{ nm}$ , where  $\Delta_p = 0 \text{ MHz}$  and other parameters are as in Fig. 2. (b) Real part  $\chi'_2$  and (d) imaginary part  $\chi''_2$  for  $T2$  trapped as an atomic lattice of a period  $a = 150 \text{ nm}$ , and here it shows the range from  $x = 60$  to  $65 \mu\text{m}$ , where  $\Delta_p = 0.1 \text{ MHz}$  and other parameters are as in Fig. 3.

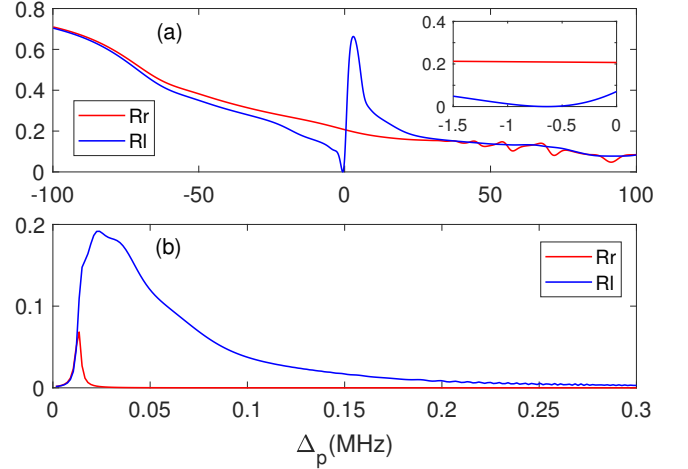


FIG. 7: Reflectivities  $R_l$  (red curves) and  $R_r$  (blue curves) against detuning  $\Delta_p$  (a) for the atomic lattice of  $T3$  and (b) the atomic lattice of  $T2$  with the same parameters corresponding to Fig. 6 (a).

As shown in Fig. 7(a) for the  $T3$  lattice, there is still one unidirectional reflectionless point, however, the nonzero reflectivity  $R_r$  can be dramatically increased by near 25 times. In the other ranges of asymmetric reflection, both the  $R_l$  and  $R_r$  can be enhanced obviously. Thus, the Bragg scattering, typically yielding symmetric reflectivities, has negligible effects on the vanishing reflectivity due to the obvious absorption based on spatial KK relation, but just enhances the nonzero reflectivity. Moreover, in the common range ( $50 \text{ MHz} < \Delta_p < 100 \text{ MHz}$ ) far from the regime of spatial KK modulation, the symmet-

ric reflections appear according to the photonic band gap arising from the atomic lattice. As shown in Fig. 7(b) for the  $T2$  lattice, there is still a unidirectional reflection range with  $R_r = 0$  but  $R_l$  of relatively large values. The the nonzero reflectivity can be increasing maximally by near 100 times. These results imply that, such a periodic spatial modulation does not obviously influence the inhomogeneous spatial KK modulation of, which is essential for developing nonreciprocal optical devices.

#### IV. CONCLUSIONS

In summary, using a well-designed atomic system of cold  $^{87}\text{Rb}$  Rydberg atoms, we have investigated the spatial KK modulation and the asymmetric reflection features induced by the position-dependent Rydberg atomic dipole-dipole interaction, either the van der Waals dipole-

dipole interaction or the Förster-like dipole-dipole exchange interaction. Via such a strong long-range interaction, we use a control atom to act on the homogeneous target atomic ensemble, and thus, the probe susceptibility of target ensemble can be modulated inhomogeneously in space. We find that the consequent position-dependent susceptibility can dynamically transfer between the regimes of the spatial KK modulation or not by adjusting the probe frequency. Then, such a tunable system can show a range or point of asymmetric and even unidirectional reflections. For enhancing the nonzero reflection, we use the Bragg scattering by trapping target atoms into the optical lattice. The nonzero reflectivity can be enhanced dramatically when the unidirectional reflection feature is still retained. This implies that the periodic spatial modulation does not hamper or spoil the main effects of the inhomogeneous spatial KK relation modulation.

- 
- [1] H. A. Haus, *Waves and fields in optoelectronics*, Prentice-Hall series in solid state physical electronics (Prentice-Hall, Englewood Cliffs and London, 1984).
  - [2] M. Greenberg and M. Orenstein, *Opt. Express* **12**, 4013 (2004).
  - [3] M. Kulishov, J. M. Laniel, N. Bélanger, J. Azaña, and D. V. Plant, *Opt. Express* **13**, 3068 (2005).
  - [4] M. Greenberg and M. Orenstein, *Opt. Lett.* **29**, 451 (2004).
  - [5] Z. Lin, H. Ramezani, T. Eichelkraut, T. Kottos, H. Cao, and D. N. Christodoulides, *Phys. Rev. Lett.* **106**, 213901 (2011).
  - [6] S. Longhi, *J. Phys. A: Math. Theor.* **44**, 485302 (2011).
  - [7] E. Yang, Y. Lu, Y. Wang, Y. Dai, and P. Wang, *Opt. Express* **24**, 14311 (2016).
  - [8] S. Kalish, Z. Lin, and T. Kottos, *Phys. Rev. A* **85**, 055802 (2012).
  - [9] A. Mostafazadeh, *Phys. Rev. A* **87**, 012103 (2013).
  - [10] Y. Huang, Y. Shen, C. Min, S. Fan, and G. Veronis, *Nanophotonics* **6**, 977 (2017).
  - [11] M. Sarisaman, *Phys. Rev. A* **95**, 013806 (2017).
  - [12] M. Sarisaman and M. Tas, *Phys. Rev. B* **97**, 045409 (2018).
  - [13] Y. Fu, Y. Xu, and H. Chen, *Opt. Express* **24**, 1648 (2016).
  - [14] N. X. A. Rivolta and B. Maes, *Phys. Rev. A* **94**, 053854 (2016).
  - [15] A. Regensburger, C. Bersch, M.-A. Miri, G. Onishchukov, D. N. Christodoulides, and U. Peschel, *Nature* **488**, 167 (2012).
  - [16] L. Feng, Y.-L. Xu, W. S. Fegadolli, M.-H. Lu, J. E. B. Oliveira, V. R. Almeida, Y.-F. Chen, and A. Scherer, *Nat. Mater.* **12**, 108 (2013).
  - [17] M.-A. Miri, P. LiKamWa, and D. N. Christodoulides, *Opt. Lett.* **37**, 764 (2012).
  - [18] W. Liu, M. Li, R. S. Guzzon, E. J. Norberg, J. S. Parker, M. Lu, L. A. Coldren, and J. Yao, *Nat. Commun.* **8**, 1 (2017).
  - [19] G. Castaldi, S. Savoia, V. Galdi, A. Alu, and N. Engheta, *Phys. Rev. Lett.* **110**, 173901 (2013).
  - [20] J. Lekner, *Am. J. Phys.* **75**, 1151 (2007).
  - [21] F. L. Teixeira and W. C. Chew, *J. Electromagn. Anal. Appl.* **13**, 665 (1999).
  - [22] L. D. Landau and E. M. Lifshits, *Quantum mechanics: Non-relativistic theory*, third edition, revised and enlarged. ed., Their Course of theoretical physics, Vol. volume 3 (Pergamon Press, Oxford and New York, 1977).
  - [23] U. Leonhardt, *Science* **312**, 1777 (2006).
  - [24] J. B. Pendry, D. Schurig, and D. R. Smith, *Science* **312**, 1780 (2006).
  - [25] S. Savoia, G. Castaldi, and V. Galdi, *J. Opt.* **18**, 044027 (2016).
  - [26] K. Sainath and F. L. Teixeira, *J. Opt. Soc. Am. B* **32**, 1645 (2015).
  - [27] M.-A. Miri, M. Heinrich, and D. N. Christodoulides, *Optica* **1**, 89 (2014).
  - [28] S. Longhi, *Opt. Lett.* **40**, 463 (2015).
  - [29] S. A. Horsley, M. Artoni, and G. C. La Rocca, *Nat. Photonics* **9**, 436 (2015).
  - [30] C. G. King, S. A. R. Horsley, and T. G. Philbin, *J. Opt.* **19**, 085603 (2017).
  - [31] S. A. R. Horsley, *Phys. Rev. A* **97** (2018).
  - [32] S. A. R. Horsley and S. Longhi, *Am. J. Phys.* **85**, 439 (2017).
  - [33] S. A. R. Horsley and S. Longhi, *Phys. Rev. A* **96** (2017).
  - [34] D. Ye, C. Cao, T. Zhou, J. Huangfu, G. Zheng, and L. Ran, *Nat. Commun.* **8**, 1 (2017).
  - [35] D. Liu, Y. Huang, H. Hu, L. Liu, D. Gao, L. Ran, D. Ye, and Y. Luo, *IEEE Trans. Antennas Propag.* **68**, 2945 (2020).
  - [36] D. Barredo, S. Ravets, H. Labuhn, L. Béguin, A. Vernier, F. Nogrette, T. Lahaye, and A. Browaeys, *Phys. Rev. Lett.* **112**, 183002 (2014).
  - [37] M. D. Lukin, M. Fleischhauer, R. Cote, L. M. Duan, D. Jaksch, J. I. Cirac, and P. Zoller, *Phys. Rev. Lett.* **87**, 037901 (2001).
  - [38] V. Lienhard, S. de Léséleuc, D. Barredo, T. Lahaye, A. Browaeys, M. Schuler, L.-P. Henry, and A. M.

- Läuchli, Phys. Rev. X **8** (2018).
- [39] H. Bernien, S. Schwartz, A. Keesling, H. Levine, A. Omran, H. Pichler, S. Choi, A. S. Zibrov, M. Endres, M. Greiner, V. Vuletić, and M. D. Lukin, Nature **551**, 579 (2017).
  - [40] M. Saffman, J. Phys. B: At. Mol. Opt. Phys. **49**, 202001 (2016).
  - [41] H. Fan, S. Kumar, J. Sedlacek, H. Kübler, S. Karimkashi, and J. P. Shaffer, J. Phys. B: At. Mol. Opt. Phys. **48**, 202001 (2015).
  - [42] M. T. Simons, A. H. Haddab, J. A. Gordon, and C. L. Holloway, Appl. Phys. Lett. **114**, 114101 (2019).
  - [43] D. H. Meyer, K. C. Cox, F. K. Fatemi, and P. D. Kunz, Appl. Phys. Lett. **112**, 211108 (2018).
  - [44] O. Firstenberg, C. S. Adams, and S. Hofferberth, Journal of Physics **49**, 152003 (2016).
  - [45] A. K. Mohapatra, T. R. Jackson, and C. S. Adams, Phys. Rev. Lett. **98**, 113003 (2007).
  - [46] Y.-M. Liu, D. Yan, X.-D. Tian, C.-L. Cui, and J.-H. Wu, Phys. Rev. A **89** (2014).
  - [47] C. S. Adams, J. D. Pritchard, and J. P. Shaffer, J. Phys. B **53**, 012002 (2020).
  - [48] C.-H. Fan, H.-X. Zhang, and J.-H. Wu, Phys. Rev. A **99** (2019).
  - [49] J.-H. Wu, M. Artoni, and G. C. La Rocca, Phys. Rev. A **92** (2015).
  - [50] Y.-M. Liu, X.-D. Tian, D. Yan, Y. Zhang, C.-L. Cui, and J.-H. Wu, Phys. Rev. A **91** (2015).
  - [51] D. Tong, S. M. Farooqi, J. Stanojevic, S. Krishnan, Y. P. Zhang, R. Côté, E. E. Eyler, and P. L. Gould, Phys. Rev. Lett. **93**, 063001 (2004).
  - [52] T. Vogt, M. Viteau, J. Zhao, A. Chotia, D. Comparat, and P. Pillet, Phys. Rev. Lett. **97**, 083003 (2006).
  - [53] D. Ma, D. Yu, X.-D. Zhao, and J. Qian, Phys. Rev. A **99** (2019).
  - [54] C. Hang, W. Li, and G. Huang, Phys. Rev. A **100** (2019).
  - [55] J. Liu, N. Liu, C. Shan, H. Li, T. Liu, and A. Zheng, J. Phys. B-At. Mol. Opt. Phys. **53**, 145401 (2020).
  - [56] Y.-M. Liu, X.-D. Tian, J. Wang, C.-H. Fan, F. Gao, and Q.-Q. Bao, Opt. Express **26**, 12330 (2018).
  - [57] H. Gorniaczyk, C. Tresp, J. Schmidt, H. Fedder, and S. Hofferberth, Phys. Rev. Lett. **113**, 053601 (2014).
  - [58] Y. M. Hao, G. W. Lin, X. M. Lin, Y. P. Niu, and S. Q. Gong, Sci Rep **9**, 4723 (2019).
  - [59] L. D. Landau, E. M. Lifshits, and L. P. Pitaevski, *Electrodynamics of continuous media*, 2nd ed., Course of theoretical physics, Vol. vol.8 (Pergamon, Oxford, 1984).
  - [60] S. A. R. Horsley, M. Artoni, and G. C. La Rocca, Phys. Rev. A **94** (2016).
  - [61] M. Artoni, G. La Rocca, and F. Bassani, Phys. Rev. E: Stat., Nonlinear, Soft Matter Phys. **72**, 046604 (2005).
  - [62] Daniel Adam Steck, “Rubidium 87 D line data,” (2019).
  - [63] J. K. Stockton, *Continuous Quantum Measurement of Cold Alkali-Atom Spins*, Ph.D. thesis, California Institute of Technology (2007).
  - [64] S. Longhi, Europhys. Lett. **112**, 64001 (2015).
  - [65] W. Jiang, Y. Ma, J. Yuan, G. Yin, W. Wu, and S. He, Laser Photonics Rev. **11**, 1600253 (2017).
  - [66] S. A. R. Horsley and S. Longhi, Phys. Rev. A **96** (2017).
  - [67] T. G. Philbin, J. Opt. **18**, 01LT01 (2016).
  - [68] S. A. R. Horsley, C. G. King, and T. G. Philbin, J. Opt. **18**, 044016 (2016).
  - [69] S. Longhi, Phys. Rev. A **96** (2017).